RSC Advances

PAPER

View Article Online
View Journal | View Issue

Cite this: *RSC Adv.*, 2022, **12**, 3119

Coating metal–organic frameworks on plasmonic Ag/AgCl nanowire for boosting visible light photodegradation of organic pollutants

Xi Chen,[a] Yanshuang Zhang,[ac] Xiangyun Kong,[a] Bowen Yu,[a] Shuaiyin Wang,[a] Wenyuan Xu,[a] Zhili Fang,[a] Jiali Zhang,[a] Kun Yao*[b] and Yongxin Liu*[a]

Received 23rd November 2021
Accepted 12th January 2022

DOI: 10.1039/d1ra08576j

rsc.li/rsc-advances

Photoactive metal–organic frameworks, MIL-100(Fe), with controllable thickness are coated on plasmonic Ag/AgCl nanowire, for boosting visible light photodegradation of rhodamine B and tetracycline hydrochloride. The morphology and composition of the obtained nano-heterostructure were investigated in detail by SEM imaging, TEM imaging, XRD patterns, FT-IR spectra, N_2 adsorption–desorption curves and TGA patterns. Photoelectric performance test suggested that a Z-scheme photocatalysis system for efficient transfer of photogenerated charge carriers was established between MIL-100(Fe) and plasmonic Ag/AgCl nanowire.

1. Introduction

With the progress of science and technology, the human living environment contains a lot of organic pollutants, especially from pesticides, dyes, leather, medicine, oil refining, metallurgy, paper, various chemical productions and wastes, *etc.*, greatly threatening human health and ecological environments.[1–3] Therefore, the efficient degradation of organic pollutants in water environment has become an important research problem in environmental treatment. The commonly used methods for degrading organic pollutants include physical methods,[4,5] advanced oxidation methods,[6,7] biological treatment methods,[8,9] electrochemical degradation,[10,11] *etc.* Particularly, photodegradation by using inorganic semiconductors such as TiO_2 and CdS benefits from low cost, no secondary pollution and high efficiency, suggesting a kind of environmentally friendly method.[12–15] However, nonporous inorganic semiconductors with low specific surface area usually present poor ability in adsorbing organic pollutants, which limits their application to a large extent. Therefore, the research and development of new high efficiency photocatalysts have become an important research direction.

In recent years, metal–organic framework materials (MOFs), assembled and extended by the coordination of organic ligands and metal ions, have become promising porous materials due to their characteristics of structure and function controllability, regular arrangement of pores and high specific surface area.[16–18] Recently, MOFs have become recognized as efficient photocatalytic materials due to the generation of charge carriers under irradiation.[19–21] For example, MOF-5,[22] ZIF-67,[23] MIL-88(A),[24] ZIF-8 (ref. 25) *etc.* have already been used in the photodegradation of organic pollutants. However, pure MOFs exhibit fast combination of electrons and holes during the catalytic process, rendering a low catalytic efficiency. Therefore, to efficiently separate electrons and holes is quite important for boosting the catalytic efficiency of MOF photocatalysts. In recent years, some methods including modification of ligands, use of multiple metal centers, doping and building composites have been adopted to promote the photocatalytic behavior of MOFs.[26–28]

Plasmonic metals including platinum (Pt) and gold (Au) are favored to promote the catalytic performance of MOFs by conducting electrons, taking advantage of the local surface plasmon resonance (SPR).[29–31] As a plasmonic metal, silver (Ag) stands out due to the high conductivity and low cost.[32–34] Particularly, AgCl is always accompanied with the presence of Ag to modify MOFs. The lifetime of photogenerated electrons is prolonged by a good matching of the energy band structure of MOFs and AgCl, and the SPR effect of Ag. Inspired by the highly efficient catalysis, a lot of Ag/AgCl/MOFs photocatalytic systems have been established to photodegrade organic pollutants, including Ag/AgCl@MIL-88A(Fe),[35–37] Ag/AgCl/NH_2-UiO-66,[38] Ag/AgCl@MIL-53-Fe,[39] ZIF-67/AgCl/Ag,[40] Ag/AgCl/NH_2-MIL-101(Fe)[41] *etc.* In these Ag/AgCl/MOFs photocatalytic systems, MOFs are excited by light radiation to produce electrons in the conduction band (CB) and holes in the valence band (VB). The electrons in the CB of MOFs transfer to the positive sites of Ag derived from the fluctuation of electrons in SPR, rendering a Z-

[a]*School of Materials Science and Engineering, East China Jiaotong University, Shuanggang Road 808, Nanchang, 330013, People's Republic of China. E-mail: liuyx629@foxmail.com*

[b]*Shenzhen Zhongxing New Material Technology Company Ltd., Shenzhen, 518000, People's Republic of China. E-mail: 381003700@qq.com*

[c]*Ganjiang Innovation Academy, Chinese Academy of Sciences, Academy of Science Road 1, Ganzhou, 341003, People's Republic of China*

scheme structure. Meanwhile, the fluctuation electrons of Ag transfer into the CB of AgCl, further prolonging the photogenerated electron lifetime and initiating reduction reaction in the reaction system.

From the perspective of nanostructures, the Ag/AgCl is coated on MOFs in the above Ag/AgCl/MOFs photocatalytic systems. To the best of our knowledge, little attention has been paid to the opposing situation, coating MOFs on Ag/AgCl, to catalyze the photodegradation of organic pollutants. Obviously, as the main component to generate photogenerated holes and electrons, MOFs can exhibit better light absorption when distributed externally. In addition, the surface of MOFs is considered as the main place where organic pollutants are degraded, not only due to the oxidizing ability of the holes in the VB of MOFs, but also because of the strong interactions between MOFs and organic pollutant molecules. Therefore, the surface effects of MOFs are expected to be enhanced without any surface covering. Inspired by these advantages, covering MOFs on plasmonic Ag/AgCl nanowire to research the photodegradation of organic pollutants represents attractive and significant work.

In this work, a MOF is uniformly coated on plasmonic Ag/AgCl nanowire to research the photodegradation of rhodamine B (Rh B) and tetracycline hydrochloride (TC·HCl). MIL-100(Fe), an Fe-based MOF built of trimesic acid (H_3btc) and Fe^{3+} ions,[42] is selected here not only due to the high activity under visible light,[43] but also because of the strong interaction between organic pollutant molecules and benzene rings on the MOF pore wall.[44] Ag nanowire is selected here as the platform on account of its unique catalytic, thermal, optical, and electronic properties.[45,46] To adjust the MOF thickness on the plasmonic Ag/AgCl nanowire, a uniform MOF coating method reported in our previous work[47] is used here. The prepared Ag/AgCl/MOFs core–shell nanowire (ACN) was characterized with detailed morphology study, component analysis and photocatalytic evaluation. A synergistic mechanism among Ag, AgCl and MOFs was proposed for boosting visible light photodegradation of organic pollutants. Moreover, the ACN series showed excellent durability.

2. Experimental

2.1 Synthesis of Ag nanowire

The synthesis of Ag nanowire was according to a previous procedure.[47] Typically, 3.5 g of 0.6 mM $FeCl_3 \cdot 6H_2O$ ethylene glycol solution was mixed with 0.2 g of polyvinylpyrrolidone, 0.25 g of $AgNO_3$ and 25 ml of ethylene glycol. The solids in the mixture were dissolved completely by magnetic stirring to form a uniform solution. The uniform solution was kept for 5 h at 130 °C. After cooling down to room temperature, the product was centrifuged and washed with ethanol three times. The final Ag nanowires were dispersed in 20 ml of ethanol.

2.2 Synthesis of Ag/AgCl nanowire

5 ml of the above Ag nanowire dispersion liquid after ultrasonic uniform dispersal was taken off immediately and added into 10 ml of $FeCl_3 \cdot 6H_2O$ ethanol solution with a concentration of 5 mM. The mixture was kept at 60 °C for 30 min to form Ag/AgCl nanowires. The Ag/AgCl nanowires were centrifuged and washed with ethanol several times.

2.3 Synthesis of ACN series

The obtained Ag/AgCl nanowire was mixed with 5 ml of $FeCl_2 \cdot 4H_2O$ aqueous solution with a concentration of 8 mM and 5 ml of aqueous solution with H_3btc concentration of 8 mM and NaOH concentration of 24 mM. The mixture was kept for 30 min at room temperature to complete one time coating of MOFs, and ACN-1 was obtained. Repeating the coating of MOFs twice and thrice, ACN-2 and ACN-3 were obtained, respectively. The obtained ACN series were centrifuged and washed with ethanol several times.

2.4 Photodegradation of Rh B

A 500 W Xe arc lamp was used to investigate the photodegradation of Rh B under visible light irradiation at 420–780 nm. Typically, 10 mg of the photocatalyst was added into 50 ml of Rh B aqueous solution with a concentration of 10 mg L^{-1}. The adsorption equilibrium was achieved by magnetic agitation for 30 min in a dark chamber. 2 ml of the photocatalytic reaction mixture was taken every 5 min, the concentration of which was determined at the maximum absorption wavelength of 554 nm with a UV-visible spectrophotometer.

2.5 Photodegradation of TC·HCl

A 500 W Xe arc lamp was used to investigate the photodegradation of TC·HCl under visible light irradiation at 420–780 nm. Typically, 10 mg of the photocatalyst was added into 50 ml of TC·HCl aqueous solution with a concentration of 50 mg L^{-1}. The adsorption equilibrium was achieved by magnetic agitation for 60 min in a dark chamber. 2 ml of the photocatalytic reaction mixture was taken every 10 min, the concentration of which was determined at the maximum absorption wavelength of 350 nm using a UV-visible spectrophotometer.

3. Results and discussion

3.1 Morphological study of ACN series

In order to facilitate the study of morphology, a schematic diagram of the morphology associated with the synthesis procedure was drawn, as illustrated in Scheme 1.

The morphology of Ag nanowires is presented *via* SEM imaging in Fig. 1a. The surface of the Ag nanowires was observed clearly to be very smooth. After reacting with $FeCl_3$, the surface of the Ag nanowires was attached with nanoparticles (Fig. 1b). HR-TEM observation suggested that both Ag and AgCl existed in the nanoparticles due to the presence of Ag lattice plane (111) with lattice distance of 0.24 nm and AgCl lattice plane (111) with lattice distance of 0.28 nm (Fig. 1c). The evolution from Ag to AgCl was contributed by the reactions between Ag and $FeCl_3$. On the one hand, $FeCl_3$ can oxidize Ag to

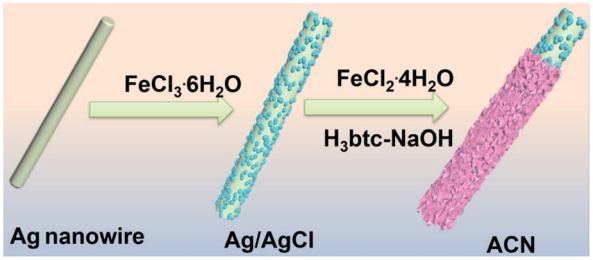

Scheme 1 Illustration of the morphology of the products associated with the synthesis procedure.

AgCl, a thermodynamically spontaneous process represented as $FeCl_3 + Ag \rightarrow FeCl_2 + AgCl$. On the other hand, AgCl decomposes in the presence of light represented as $2AgCl + h\nu \rightarrow 2Ag + Cl_2\uparrow$. Under the combination of these two reactions, AgCl was produced; meanwhile, a portion of Ag migrated from the Ag nanowire to the nanoparticles. Thus, the plasmonic Ag/AgCl nanowire is not only a good electron transfer system, but also a structured platform for MOF coating.

After coating the MOF on the Ag/AgCl nanowire, ACN was obtained. The crystals of the MOF were arranged densely on the surface of the nanowire, forming a uniform coating layer (Fig. 2a). The thickness of the MOF coating layer increases with increasing coating time during the preparation process. TEM images showed three different samples of ACN-1 (Fig. 2b), ACN-2 (Fig. 2c) and ACN-3 (Fig. 2d) with MOF coating layer thickness of about 100 nm, 150 nm and 200 nm, respectively. The nanoparticles containing Ag and AgCl were sandwiched between the Ag nanowire and the MOF coating layer. The distribution of elements evaluated by TEM-EDX further exhibited the structure and components of the core–shell hybrid material (Fig. 2e–i): Ag and Cl centered in the core area, while Fe, C and O spread all over the sheath area, rendering plasmonic Ag/AgCl nanowire core with MOF sheath.

3.2 Chemical and physical properties of ACN series

To identify the crystal phase of ACN, XRD patterns of the products were obtained. From the observation of Fig. 3a, the peaks of plasmonic Ag/AgCl nanowire, ACN-1, ACN-2 and ACN-3 well matched those of standard AgCl (JCPDS no. 31-1238) and Ag (JCPDS no. 04-0783), suggesting the crystal components. In addition, there were relatively weak peaks below 25° present in the XRD patterns of ACN-1, ACN-2 and ACN-3, which were observed to be associated with MIL-100(Fe) by magnifying the view of the XRD patterns below 25° (Fig. 3b). The obvious peaks at 11° (428) and 20.1° (4814) corresponded to the intrinsic MIL-100(Fe) crystals as reported previously.[48] Moreover, FT-IR spectra demonstrated the successful coating of MOFs on the plasmonic Ag/AgCl nanowire (Fig. 3c). Peaks at 760 cm^{-1} and 710 cm^{-1} are in the fingerprint region, associated with the C–H vibration of benzene ring. The asymmetric and symmetric vibration peaks of $-COO^-$ are present at 1625 cm^{-1} and 1375 cm^{-1}, respectively. A bridging coordination between oxygen atoms of btc^{3-} ligand and Fe^{3+} with the mode of μ_2-η^1, η^1 was proven.[49]

The BET surface areas of plasmonic Ag/AgCl nanowire, ACN-1, ACN-2 and ACN-3 are 9.36 $m^2\ g^{-1}$, 126.57 $m^2\ g^{-1}$, 161.63 $m^2\ g^{-1}$ and 206.23 $m^2\ g^{-1}$, respectively. With the thickness of the MOF layer increasing, the BET surface area of the hybrid increased, contributed by the mesopore structure and large specific area of the MOF. As illustrated in Fig. 4a, the N_2 adsorption–desorption isotherms of ACN-1, ACN-2 and ACN-3 present type I and type IV behavior, suggesting the presence of multilevel pores. Moreover, the H_3 and H_4 hysteresis loop mode indicated that the MOF coating layer is assembled of the aggregated crystals of the MOF. The thermogravimetric analysis (TGA) curves also identified the components of ACN series. From the observation of Fig. 4b, the weight loss in the first step before 120 °C is related to the release of guest molecules on the outer surface or in the pores of the MOF. The weight loss in the second step beginning at approximately 380 °C is associated with decomposition of the MOF. Accordingly, the second step weight loss percentage increased with the thickness of MOF coating layer increasing. In addition, no obvious weight loss was observed for the plasmonic Ag/AgCl nanowire before 800 °C.

3.3 Photocatalytic activities of ACN series

Rh B, a typical organic dye, and TC·HCl, a typical antibiotic, were selected here as degradation models to investigate the photocatalytic activities of ACN. From the observation of Fig. 5a, after 30 min of dark adsorption, the decrease of Rh B concentration due to adsorption is different according to the surface

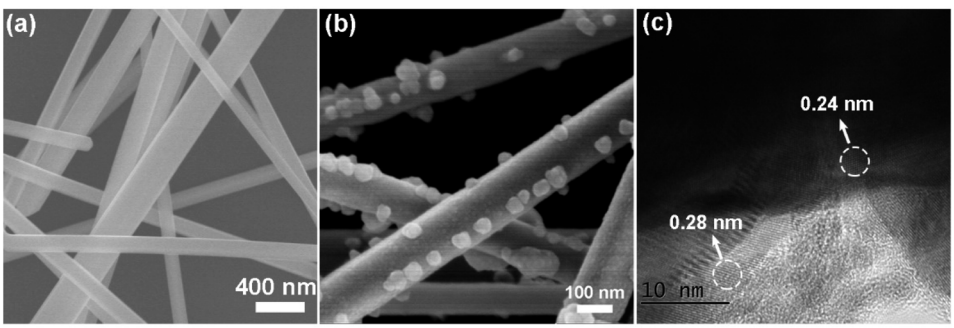

Fig. 1 SEM images of (a) Ag nanowire and (b) Ag/AgCl nanowire and (c) HR-TEM image of Ag/AgCl nanowire.

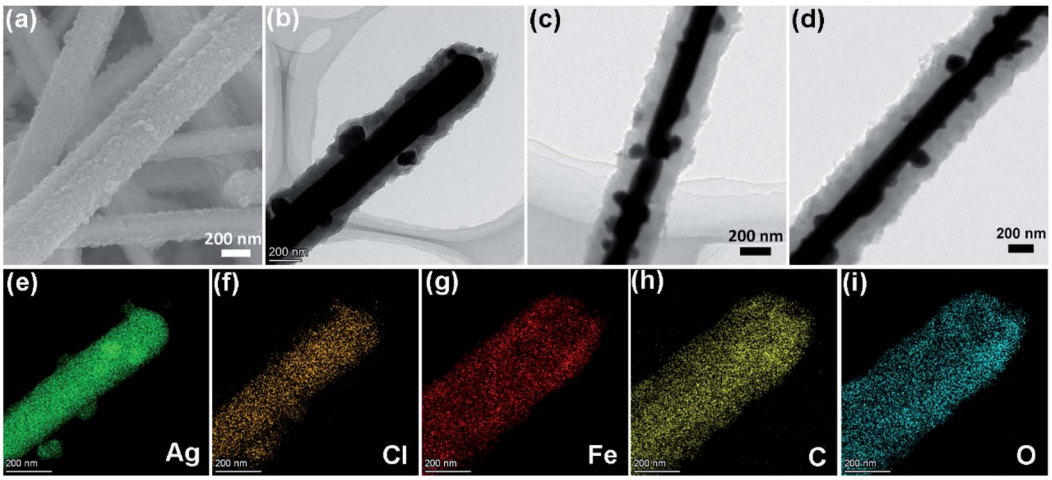

Fig. 2 (a) SEM image of ACN-2. TEM images of (b) ACN-1, (c) ACN-2 and (d) ACN-3. (e–i) TEM-EDX mapping images of ACN-1.

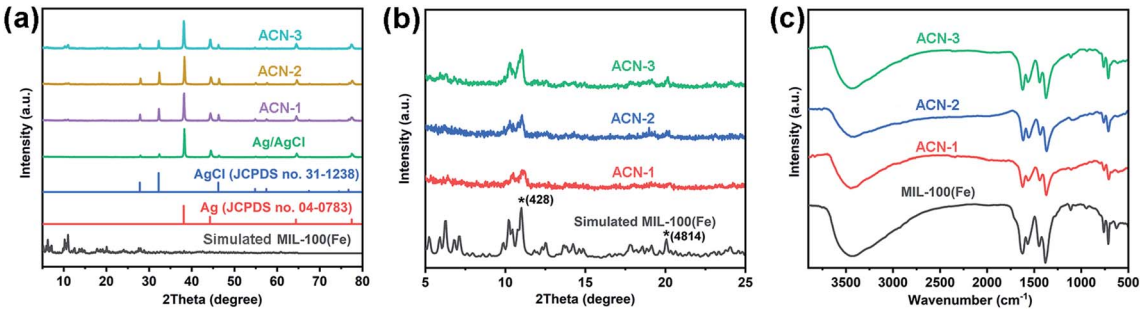

Fig. 3 (a and b) XRD patterns of simulated MIL-100(Fe), standard Ag and AgCl, plasmonic Ag/AgCl nanowire, ACN-1, ACN-2 and ACN-3. (c) FT-IR spectra of pure MOF, ACN-1, ACN-2 and ACN-3.

properties of the catalysts. There is almost no adsorption of Rh B on Ag and Ag/AgCl nanowires because of the low specific surface area. However, coating with MOF enhanced the dark adsorption of Rh B due to the high specific surface area and the strong intermolecular forces between the MOF and Rh B. The equilibrium adsorption capacity of Rh B increased with increasing amount of MOF coating layer on the surface of Ag/AgCl nanowire, which is in accordance with our previous work.[50] Under visible light irradiation, Rh B degraded immediately under the catalysis of ACN-1, ACN-2 and ACN-3. However, Ag nanowires have little catalytic activity. Although the degradation of Rh B could be observed under the catalysis of

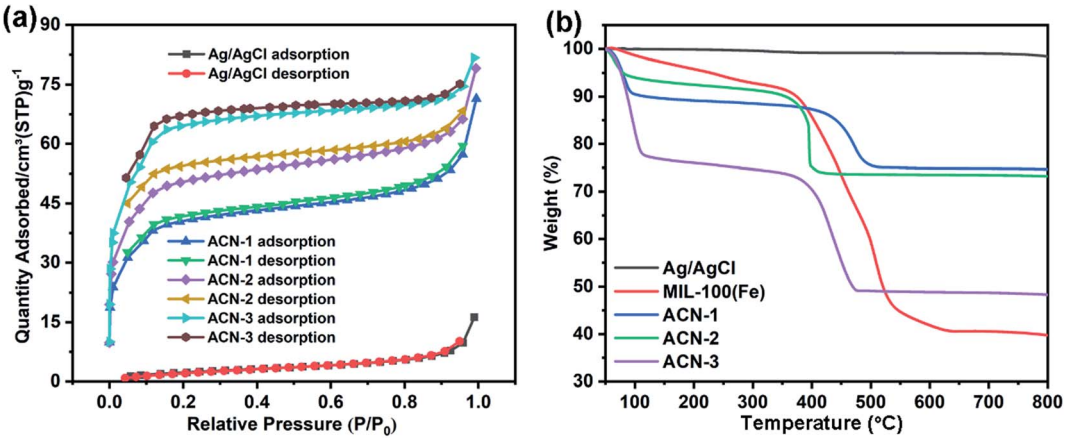

Fig. 4 (a) N_2 adsorption–desorption curves and (b) TGA patterns of plasmonic Ag/AgCl nanowire, pure MOF, ACN-1, ACN-2 and ACN-3.

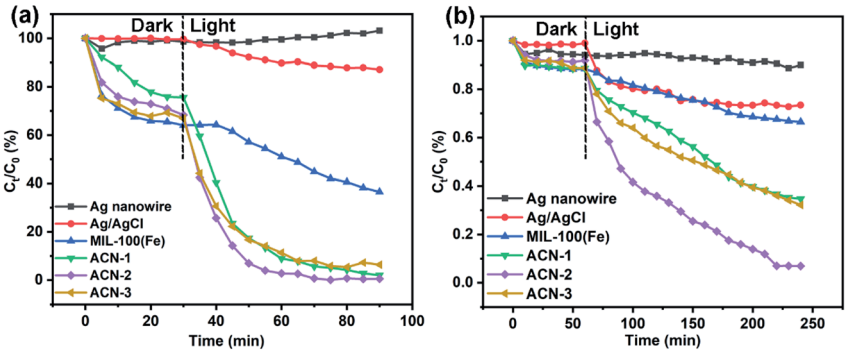

Fig. 5 Photocatalytic degradation of (a) Rh B and (b) TC·HCl using different catalysts.

Ag/AgCl nanowires and pure MOF, the trend towards Rh B degradation is not encouraging. Obviously, coating of the MOF on Ag/AgCl nanowire could boost the photocatalytic activity. The boosting is from the mutual effect among Ag, AgCl and MOF, possibly including the optical excitation of the MOF, plasmonic response of Ag nanowire and the corresponding electron transfer on AgCl. Moreover, the thickness of the MOF coating layer has an effect on the photocatalytic activity. ACN-2 showed the highest catalytic activity and a near complete degradation of Rh B was reached after 75 min. An appropriate coating thickness of MOF can harmonize the Ag SPR, electron transfer ability on AgCl, the Rh B adsorption and the optical excitation of the MOF, which promotes the charge separation efficiency. The degradation tendency of TC·HCl is similar to that of Rh B under the different catalysts (Fig. 5b). The fastest degradation rate occurred for ACN-2, a degradation of about 93% being achieved after 220 min.

A kinetic study based on the Langmuir–Hinshelwood model of photodegradation of Rh B and TC·HCl using different catalysts suggested that the degradation kinetics data could be fitted with pseudo-first-order kinetic equation of $\ln(C_0/C_t) = kt$, where C_0 and C_t are the initial concentration after the dark adsorption and the concentration at any time t after catalyst addition into the mixture solution, and k is the apparent rate constant. As illustrated in Fig. 6a and b, the kinetic rate constants k in the photodegradation of Rh B are 0.068 min^{-1}, 0.107 min^{-1} and 0.060 min^{-1} for ACN-1, ACN-2 and ACN-3, respectively. The kinetic rate constants k in the photodegradation of TC·HCl are 0.005 min^{-1}, 0.014 min^{-1} and 0.006 min^{-1} for ACN-1, ACN-2 and ACN-3, respectively. To investigate the durability, five cycles of the photodegradation of Rh B and TC·HCl were

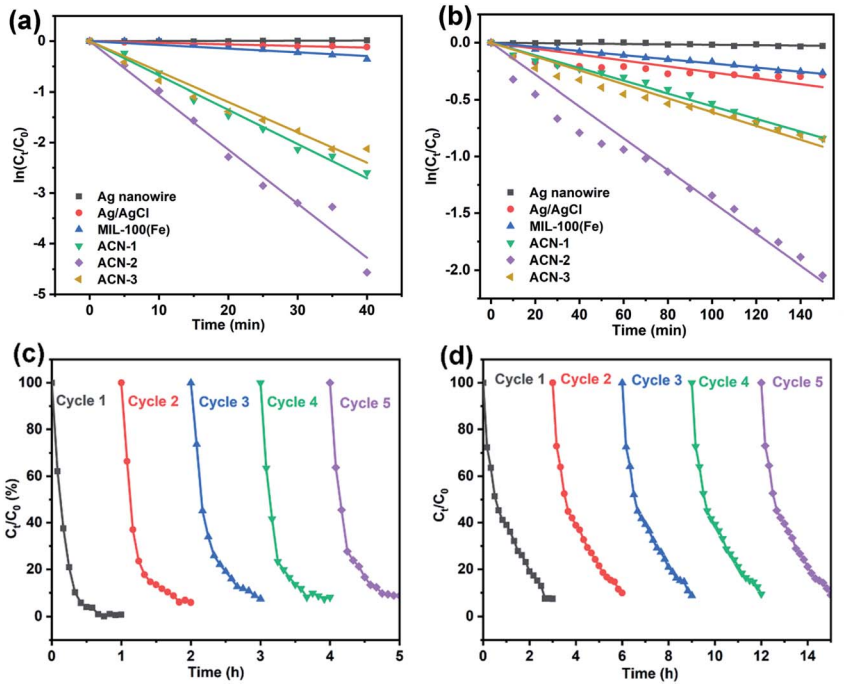

Fig. 6 Kinetics study of the degradation of (a) Rh B and (b) TC·HCl. Durability test of ACN-2 in the photocatalytic degradation of (c) Rh B and (d) TC·HCl.

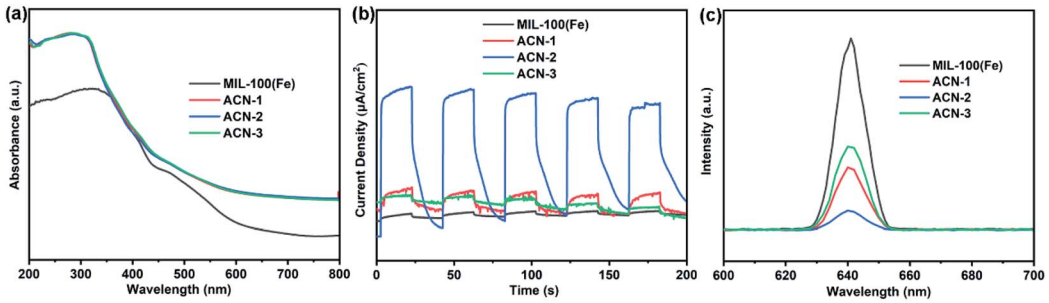

Fig. 7 (a) UV-visible diffuse reflection spectra, (b) transient photocurrent responses and (c) PL spectra of pure MOF, ACN-1, ACN-2 and ACN-3.

conducted by taking ACN-2 as the catalyst. From the observation of Fig. 6c and d, the degradation rate of Rh B and TC·HCl remained at about 91.3% and 91.0%, respectively, after five catalytic cycles.

3.4 Photoelectric performance of ACN series

To investigate the photoexcitation of the ACN series, UV-visible diffuse reflection spectra (DRS) were obtained. As illustrated in Fig. 7a, pure MOF DRS was similar to the typical DRS reported previously.[51] In contrast to the pure MOF, the ACN series have an obvious promotion in both visible light and UV absorption, which is ascribed to the SPR absorption of Ag at wavelengths above 400 nm and the excitation of AgCl at wavelengths below 400 nm, respectively.[52]

To evaluate the photoinduced electron and hole separation and migration efficiency, transient photocurrent response of the catalysts was measured (Fig. 7b). It could be observed obviously that the photocurrent response of the ACN series is higher than that of the pure MOF in several off–on cycles of visible light irradiation. As is well known, the higher the photocurrent density, the slower the photoinduced charge carrier recombination. Therefore, more efficient charge separation efficiency is obtained through the combination of Ag, AgCl and MOF. Interestingly, ACN-2 displayed the highest photocurrent density, which was in accordance with the results of organic pollutant photodegradation tests.

In addition, this result could be further evidenced by photoluminescence (PL) tests. Under excitation at 320 nm wavelength, a band between 620 and 660 nm was presented by the MOF with a 645 nm peak (Fig. 7c). In addition, it could be observed that the PL intensities followed the order of ACN-2 < ACN-1 < ACN-3 < pure MOF. A lower intensity of PL usually suggests a lower recombination rate of holes and electrons. Therefore, it could be concluded that the order of the charge separation efficiency is ACN-2 > ACN-1 > ACN-3 > pure MOF. The close interface contact through coating the MOF on Ag/AgCl nanowire facilitated the separation of photogenerated electrons and holes. What is more, the MOF coating layer with an appropriate thickness could optimize this tendency, which may have something to do with the photoexcitation of the MOF, SPR response of Ag, or charge transfer based on the interface issue of AgCl. Obviously, ACN-2 has the most appropriate thickness of the MOF coating layer in this ACN series.

3.5 Proposed mechanism

Ethylenediaminetetraacetic acid disodium salt (EDTA-2Na), tetrachloromethane (CCl_4), *p*-benzoquinone (*p*-BQ) and tertiary butanol (TBA) were used as scavengers for holes, electrons, superoxide radical ($^{\bullet}O_2^-$) and hydroxyl radical ($^{\bullet}OH$), respectively, to investigate the main radical species involved in the photocatalytic reaction. From the observation of Fig. 8a, EDTA-2Na and *p*-BQ hinder obviously the degradation of Rh B, while CCl_4 and TBA hardly affect the photodegradation of Rh B. Therefore, it could be concluded that holes and $^{\bullet}O_2^-$ are of crucial importance for the photodegradation of Rh B. The CB, VB and bandgap of the MOF are about −0.53, 2.10 and 2.63 eV (*vs.* NHE), respectively, calculated according to Mott–Schottky plots and bandgap energy (Fig. 8b and c). Obviously, the MOF

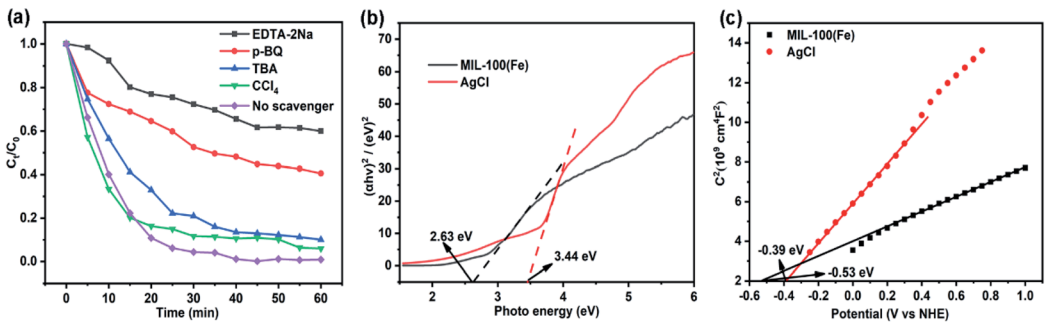

Fig. 8 (a) Scavenger influences on the photodegradation of Rh B. (b) Bandgaps and (c) Mott–Schottky plots of MOF and AgCl.

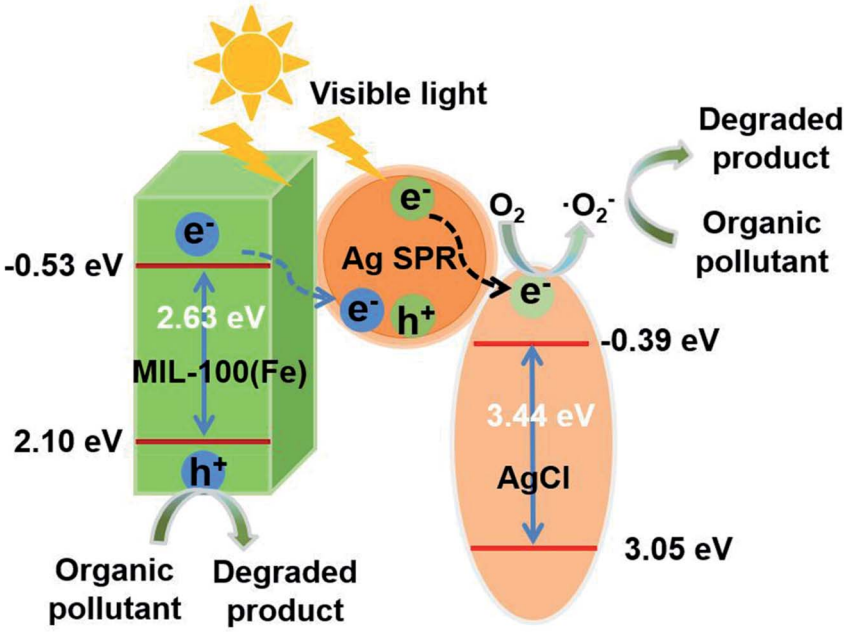

Fig. 9 Illustration of photodegradation of organic pollutants over the ACN series under visible light irradiation.

could be excited by visible light. Moreover, the CB, VB and bandgap of AgCl are about −0.39, 3.05 and 3.44 eV, respectively.

In consideration of the above discussion, the mechanism of action of the ACN series in the photodegradation of organic pollutants is proposed (Fig. 9). On the one hand, electrons from Ag SPR transfer to the AgCl CB due to the larger work function of Ag and corresponding positive centers are left in Ag. On the other hand, the MOF is photoexcited to produce holes and electrons under the irradiation of visible light. The electrons produced by the MOF could be captured immediately by the positive centers in Ag, thus establishing a Z-scheme photocatalytic process. In addition, the electrons in the AgCl CB transfer to O_2 to generate $^{\bullet}O_2^-$. Therefore, the organic pollutants could be degraded by both the holes of the MOF and $^{\bullet}O_2^-$.

4. Conclusions

MOF was uniformly coated on plasmonic Ag/AgCl nanowire to build photocatalysts (ACN series) with boosted activity for the photodegradation of organic pollutants. As the main catalyst, the MOF not only concentrated the organic pollutant molecules through its inherent pores filled with benzene pore walls, but also afforded photogenerated charge carriers to degrade the organic pollutants. As the cocatalyst, Ag/AgCl transferred electrons from MOF to O_2, prolonging the photogenerated charge carrier lifetime and producing active $^{\bullet}O_2^-$ to degrade the organic pollutants.

Conflicts of interest

There are no conflicts to declare.

Acknowledgements

This research was supported by the National Natural Science Foundation of China [21865010, 21865009, 21872049] and the Youth Science Fund of Jiangxi Province [20202BABL213023, 20212BAB203006]. The authors would like to thank Yao Tian from Shiyanjia Lab (www.shiyanjia.com) for the BET analysis.

Notes and references

1 P. Amoatey and M. S. Baawain, Effects of pollution on freshwater aquatic organisms, *Water Environ. Res.*, 2019, **91**, 1272–1287.
2 V. Katheresan, J. Kansedo and S. Y. Lau, Efficiency of various recent wastewater dye removal methods: a review, *J. Environ. Chem. Eng.*, 2018, **6**, 4676–4697.
3 R. Hao, X. Xiao, X. Zuo, J. Nan and W. Zhang, Efficient adsorption and visible-light photocatalytic degradation of tetracycline hydrochloride using mesoporous BiOI microspheres, *J. Hazard. Mater.*, 2012, **209–210**, 137–145.
4 W. Qiu, M. Vakili, G. Cagnetta, J. Huang and G. Yu, Effect of high energy ball milling on organic pollutant adsorption properties of chitosan, *Int. J. Biol. Macromol.*, 2020, **148**, 543–549.
5 W. Liu, X. Jiang and X. Chen, A novel method of synthesizing cyclodextrin grafted multiwall carbon nanotubes/iron oxides and its adsorption of organic pollutant, *Appl. Surf. Sci.*, 2014, **320**, 764–771.
6 M. Gągol, A. Przyjazny and G. Boczkaj, Wastewater treatment by means of advanced oxidation processes based on cavitation – a review, *Chem. Eng. J.*, 2018, **338**, 599–627.
7 M. Li, Z. Qiang, P. Hou, J. R. Bolton, J. Qu, P. Li and C. Wang, VUV/UV/Chlorine as an Enhanced Advanced Oxidation

Process for Organic Pollutant Removal from Water: Assessment with a Novel Mini-Fluidic VUV/UV Photoreaction System (MVPS), *Environ. Sci. Technol.*, 2016, **50**, 5849–5856.

8 C. Grandclément, I. Seyssiecq, A. Piram, P. Wong-Wah-Chung, G. Vanot, N. Tiliacos, N. Roche and P. Doumenq, From the conventional biological wastewater treatment to hybrid processes, the evaluation of organic micropollutant removal: a review, *Water Res.*, 2017, **111**, 297–317.

9 H. Liu, Y.-h. He, X.-c. Quan, Y.-x. Yan, X.-h. Kong and A.-j. Lia, Enhancement of organic pollutant biodegradation by ultrasound irradiation in a biological activated carbon membrane reactor, *Process Biochem.*, 2005, **40**, 3002–3007.

10 V. K. Gupta, R. Jain and S. Varshney, Electrochemical removal of the hazardous dye Reactofix Red 3 BFN from industrial effluents, *J. Colloid Interface Sci.*, 2007, **312**, 292–296.

11 P. Su, M. Zhou, X. Lu, W. Yang, G. Ren and J. Cai, Electrochemical catalytic mechanism of N-doped graphene for enhanced H_2O_2 yield and in situ degradation of organic pollutant, *Appl. Catal., B*, 2019, **245**, 583–595.

12 W. S. Nam and G. Y. Han, Characterization and photocatalytic performance of nanosize TiO_2 powders prepared by the solvothermal method, *Korean J. Chem. Eng.*, 2003, **20**, 1149–1153.

13 M. Wang, J. Ioccozia, L. Sun, C. Lin and Z. Lin, Inorganic-modified semiconductor TiO_2 nanotube arrays for photocatalysis, *Energy Environ. Sci.*, 2014, **7**, 2182–2202.

14 H. Wei, L. Wang, Z. Li, S. Ni and Q. Zhao, Synthesis and Photocatalytic Activity of One-Dimensional CdS@TiO_2 Core-Shell Heterostructures, *Nano-Micro Lett.*, 2011, **3**, 6–11.

15 Z. L. Fang, H. F. Rong, Z. L. Ya and P. Qi, In situ synthesis of CdS/g-C_3N_4 hybrid nanocomposites with enhanced visible photocatalytic activity, *J. Mater. Sci.*, 2015, **50**, 3057–3064.

16 J. R. Long and O. M. Yaghi, The pervasive chemistry of metal–organic frameworks, *Chem. Soc. Rev.*, 2009, **38**, 1213–1214.

17 H.-C. Zhou, J. R. Long and O. M. Yaghi, Introduction to Metal–Organic Frameworks, *Chem. Rev.*, 2012, **112**, 673–674.

18 H.-C. J. Zhou and S. Kitagawa, Metal–Organic Frameworks (MOFs), *Chem. Soc. Rev.*, 2014, **43**, 5415–5418.

19 Q. Wang, Q. Gao, A. M. Al-Enizi, A. Nafady and S. Ma, Recent advances in MOF-based photocatalysis: environmental remediation under visible light, *Inorg. Chem. Front.*, 2020, **7**, 300–339.

20 J. Guo, Y. Wan, Y. Zhu, M. Zhao and Z. Tang, Advanced photocatalysts based on metal nanoparticle/metal-organic framework composites, *Nano Res.*, 2021, **14**, 2037–2052.

21 J.-D. Xiao and H.-L. Jiang, Metal–Organic Frameworks for Photocatalysis and Photothermal Catalysis, *Acc. Chem. Res.*, 2019, **52**, 356–366.

22 M. Alvaro, E. Carbonell, B. Ferrer, F. X. LlabrésiXamena and H. Garcia, Semiconductor Behavior of a Metal-Organic Framework (MOF), *Chem.–Eur. J.*, 2007, **13**, 5106–5112.

23 H. Yang, X.-W. He, F. Wang, Y. Kang and J. Zhang, Doping copper into ZIF-67 for enhancing gas uptake capacity and visible-light-driven photocatalytic degradation of organic dye, *J. Mater. Chem.*, 2012, **22**, 21849–21851.

24 W.-T. Xu, L. Ma, F. Ke, F.-M. Peng, G.-S. Xu, Y.-H. Shen, J.-F. Zhu, L.-G. Qiu and Y.-P. Yuan, Metal–organic frameworks MIL-88A hexagonal microrods as a new photocatalyst for efficient decolorization of methylene blue dye, *Dalton Trans.*, 2014, **43**, 3792–3798.

25 H.-P. Jing, C.-C. Wang, Y.-W. Zhang, P. Wang and R. Li, Photocatalytic degradation of methylene blue in ZIF-8, *RSC Adv.*, 2014, **4**, 54454–54462.

26 L. Shen, R. Liang and L. Wu, Strategies for engineering metal-organic frameworks as efficient photocatalysts, *Chin. J. Catal.*, 2015, **36**, 2071–2088.

27 D. Jiang, P. Xu, H. Wang, G. Zeng, D. Huang, M. Chen, C. Lai, C. Zhang, J. Wan and W. Xue, Strategies to improve metal organic frameworks photocatalyst's performance for degradation of organic pollutants, *Coord. Chem. Rev.*, 2018, **376**, 449–466.

28 S. Tasleem, M. Tahir and W. A. Khalifa, Current trends in structural development and modification strategies for metal-organic frameworks (MOFs) towards photocatalytic H_2 production: a review, *Int. J. Hydrogen Energy*, 2021, **46**, 14148–14189.

29 S.-S. Wang, L. Jiao, Y. Qian, W.-C. Hu, G.-Y. Xu, C. Wang and H.-L. Jiang, Boosting Electrocatalytic Hydrogen Evolution over Metal–Organic Frameworks by Plasmon-Induced Hot-Electron Injection, *Angew. Chem., Int. Ed.*, 2019, **58**, 10713–10717.

30 S. Li, P. Miao, Y. Zhang, J. Wu, B. Zhang, Y. Du, X. Han, J. Sun and P. Xu, Recent Advances in Plasmonic Nanostructures for Enhanced Photocatalysis and Electrocatalysis, *Adv. Mater.*, 2021, **33**, 2000086.

31 M. Wang, Y. Tang and Y. Jin, Modulating Catalytic Performance of Metal–Organic Framework Composites by Localized Surface Plasmon Resonance, *ACS Catal.*, 2019, **9**, 11502–11514.

32 B. J. Wiley, S. H. Im, Z.-Y. Li, J. McLellan, A. Siekkinen and Y. Xia, Maneuvering the Surface Plasmon Resonance of Silver Nanostructures through Shape-Controlled Synthesis, *J. Phys. Chem. B*, 2006, **110**, 15666–15675.

33 C. Duan, C. Liu, X. Meng, K. Gao, W. Lu, Y. Zhang, L. Dai, W. Zhao, C. Xiong, W. Wang, Y. Liu and Y. Ni, Facile synthesis of Ag NPs@ MIL-100(Fe)/guar gum hybrid hydrogel as a versatile photocatalyst for wastewater remediation: Photocatalytic degradation, water/oil separation and bacterial inactivation, *Carbohydr. Polym.*, 2020, **230**, 115642.

34 K. Awazu, M. Fujimaki, C. Rockstuhl, J. Tominaga, H. Murakami, Y. Ohki, N. Yoshida and T. Watanabe, A Plasmonic Photocatalyst Consisting of Silver Nanoparticles Embedded in Titanium Dioxide, *J. Am. Chem. Soc.*, 2008, **130**, 1676–1680.

35 W. Huang, C. Jing, X. Zhang, M. Tang, L. Tang, M. Wu and N. Liu, Integration of plasmonic effect into spindle-shaped MIL-88A(Fe): steering charge flow for enhanced visible-light photocatalytic degradation of ibuprofen, *Chem. Eng. J.*, 2018, **349**, 603–612.

36 V. P. Viswanathan, K. S. Divya, D. P. Dubal, N. N. Adarsh and S. Mathew, Ag/AgCl@MIL-88A(Fe) heterojunction ternary composites: towards the photocatalytic degradation of organic pollutants, *Dalton Trans.*, 2021, **50**, 2891–2902.

37 W. Wu, J. Wang, T. Zhang, S. Jiang, X. Ma, G. Zhang, X. Zhang, X. Chen and B. Li, Controllable synthesis of Ag/AgCl@MIL-88A via in situ growth method for morphology-dependent photocatalytic performance, *J. Mater. Chem. C*, 2019, **7**, 5451–5460.

38 W. Zhao, T. Ding, Y. Wang, M. Wu, W. Jin, Y. Tian and X. Li, Decorating Ag/AgCl on UiO-66-NH_2: synergy between Ag plasmons and heterostructure for the realization of efficient visible light photocatalysis, *Chin. J. Catal.*, 2019, **40**, 1187–1197.

39 Q. Liu, C. Zeng, L. Ai, Z. Hao and J. Jiang, Boosting visible light photoreactivity of photoactive metal-organic framework: designed plasmonic Z-scheme Ag/AgCl@MIL-53-Fe, *Appl. Catal., B*, 2018, **224**, 38–45.

40 W. Shao, Y.-R. Chen, F. Xie, H. Zhang, H.-T. Wang and N. Chang, Facile construction of a ZIF-67/AgCl/Ag heterojunction via chemical etching and surface ion exchange strategy for enhanced visible light driven photocatalysis, *RSC Adv.*, 2020, **10**, 38174–38183.

41 C. Xu, Design and preparation of Ag/AgCl/NH_2-MIL-101 (Fe) ternary composite photocatalysts with visible light application prospects, *IOP Conf. Ser. Earth Environ. Sci.*, 2020, **615**, 012121.

42 P. Horcajada, S. Surblé, C. Serre, D.-Y. Hong, Y.-K. Seo, J.-S. Chang, J.-M. Grenèche, I. Margiolaki and G. Férey, Synthesis and catalytic properties of MIL-100(Fe), an iron(iii) carboxylate with large pores, *Chem. Commun.*, 2007, 2820–2822, DOI: 10.1039/B704325B.

43 Y. Fang, Z. Yang, H. Li and X. Liu, MIL-100(Fe) and its derivatives: from synthesis to application for wastewater decontamination, *Environ. Sci. Pollut. Res.*, 2020, **27**, 4703–4724.

44 F. Tan, M. Liu, K. Li, Y. Wang, J. Wang, X. Guo, G. Zhang and C. Song, Facile synthesis of size-controlled MIL-100(Fe) with excellent adsorption capacity for methylene blue, *Chem. Eng. J.*, 2015, **281**, 360–367.

45 Y. Xia, P. Yang, Y. Sun, Y. Wu, B. Mayers, B. Gates, Y. Yin, F. Kim and H. Yan, One-Dimensional Nanostructures: Synthesis, Characterization, and Applications, *Adv. Mater.*, 2003, **15**, 353–389.

46 J. Chen, B. J. Wiley and Y. Xia, One-Dimensional Nanostructures of Metals: Large-Scale Synthesis and Some Potential Applications, *Langmuir*, 2007, **23**, 4120–4129.

47 X. Chen, Y. Zhang, X. Kong, Z. Guo, W. Xu, Z. Fang, S. Wang, L. Liu, Y. Liu and J. Zhang, Controlling crystal growth of MIL-100(Fe) on Ag nanowire surface for optimizing catalytic performance, *RSC Adv.*, 2020, **10**, 25260–25265.

48 C.-F. Zhang, L.-G. Qiu, F. Ke, Y.-J. Zhu, Y.-P. Yuan, G.-S. Xu and X. Jiang, A novel magnetic recyclable photocatalyst based on a core–shell metal–organic framework Fe_3O_4@MIL-100(Fe) for the decolorization of methylene blue dye, *J. Mater. Chem. A*, 2013, **1**, 14329–14334.

49 J.-L. Zhuang, M. Kind, C. M. Grytz, F. Farr, M. Diefenbach, S. Tussupbayev, M. C. Holthausen and A. Terfort, Insight into the Oriented Growth of Surface-Attached Metal–Organic Frameworks: Surface Functionality, Deposition Temperature, and First Layer Order, *J. Am. Chem. Soc.*, 2015, **137**, 8237–8243.

50 Y. Liu, S. Wang, Y. Lu, Y. Zhao, Y. Zhang, G. Xu, J. Zhang, Z. Fang, W. Xu and X. Chen, Loading Control of Metal–Organic Frameworks in Fe_3O_4@MOFs Series Composite Adsorbents for Optimizing Dye Adsorption, *Ind. Eng. Chem. Res.*, 2019, **58**, 22244–22249.

51 K. G. M. Laurier, F. Vermoortele, R. Ameloot, D. E. De Vos, J. Hofkens and M. B. J. Roeffaers, Iron(III)-Based Metal–Organic Frameworks As Visible Light Photocatalysts, *J. Am. Chem. Soc.*, 2013, **135**, 14488–14491.

52 R. Dong, B. Tian, C. Zeng, T. Li, T. Wang and J. Zhang, Ecofriendly Synthesis and Photocatalytic Activity of Uniform Cubic Ag@AgCl Plasmonic Photocatalyst, *J. Phys. Chem. C*, 2013, **117**, 213–220.